Magn Reson Med Sci 2021; 20; 216–221
doi:10.2463/mrms.tn.2020-0014
Published Online: July 8, 2020

TECHNICAL NOTE

Efficacy of a Nonrigid Image-registration Method in Comparison to Readout-segmented Echo-planar Imaging for Correcting Distortion in Diffusion-weighted Imaging

Takuya Kobata*, Tatsuya Yamasaki, Hiroki Katayama, and Kazuo Ogawa

We evaluated the effectiveness of distortion correction using a nonrigid image registration method in diffusion-weighted imaging, comparing it with readout-segmented echo planar imaging (RS-EPI). Unlike the RS-EPI, the effectiveness of the distortion correction of the nonrigid registration method depended on the slice level, being most accurate at the level of the basal ganglia, lateral ventricle, and centrum semiovale.

Keywords: *diffusion-weighted imaging, nonrigid image registration, echo planar imaging, brain, readout segmented echo planar imaging*

Introduction

Diffusion-weighted image (DWI) plays an important role in MRI. It has high sensitivity and specificity for detecting acute stroke, and distinguishing it from other diseases.[1] Generally, echo planar imaging (EPI) is used for DWI. Image distortion often occurs due to both local magnetic field inhomogeneities and eddy current effects that arise from motion-probing gradients.

Recently, distortion reduction using readout segmented-EPI (RS-EPI) DWI for clinical diagnosis has been reported.[2] RS-EPI performs signal acquisition by dividing *k*-space in the readout direction, allowing reduction of echo space to reduce the image distortion caused by phase-dephasing.[3] However, the scan time of RS-EPI DWI is longer than that of single shot-EPI (SS-EPI) DWI, and moreover, RS-EPI DWI is not available in all MRI scanners at present. Here, the nonrigid image registration method proposed by Ardekani and Sinha,[4] which is a post-processing method that corrects the distortion of the *b*0 images using T_2-weighted image (T_2WI) as reference, can be a solution for these problems. This is because the proposed method does not elongate the scan time and does not require a special MRI scanner as it is a post-processing for the scanned images. However, the effectiveness of the non-rigid image registration compared with RS-EPI DWI in regard of distortion correction is not yet reported. The purpose of this study was to evaluate the effectiveness of a nonrigid image registration compared to RS-EPI DWI for correcting the distortion in DWI.

Department of Radiology, Kagawa University Hospital, Kagawa, Japan

*Corresponding author: Department of Radiology, Kagawa University Hospital, 1750-1, Ikenobe, Mikicho, Kita-gun, Kagawa 761-0793, Japan. Phone: +81-87-898-5111, Fax: +81-87-898-2351, E-mail: kobakoba@med.kagawa-u.ac.jp

Received: January 23, 2020 | Accepted: May 9, 2020

Materials and Methods

MRI scans

This study protocol was approved by the Institutional Review Board of Kagawa University. Seven healthy volunteers (age: 31 ± 0.5 years) with no history of brain tumor or cerebrovascular disease were enrolled in this study. Informed consent was obtained from all individual participants included in the study. MR brain imaging was performed with a 3T scanner (MAGNETOM Skyra 3T; Siemens Healthcare, Erlangen, Germany) with a 20-channel head coil. Scan parameters of each sequence are shown in Table 1. DWI was obtained using SS-EPI and RS-EPI sequences. Fast spin-echo T_2WI (FSE-T_2WIs) was obtained as the reference image for the nonrigid image registration. The scanning plane of each MR image was set parallel to the anterior–posterior commissural (AC-PC) line (Fig. 1). For each subject, the scanning range was set so that the brainstem was included in slice numbers 1–10. In the RS-EPI DWI, the shortest echo space was 0.3 ms, which was achieved by setting the number of segments to 5.

Extraction of brain regions from each MR image

Figure 2 shows the schematics for extraction of brain regions from the images. Fiji software (version 2.0.0-rc-69/1.52p; National Institutes of Health, Bethesda, MD, USA) was used for this purpose.[5] First, to create mask images, local thickness-processing was performed on each slice.[6] The pixel value of the image after this processing depended on the thicknesses of the structures. Next, a radiological technologist manually set a threshold value within the range of 20–50 for each MR image to separate brain regions from other tissue, and confirmed the

Table 1 Scan parameters of each MRI sequence

Scan parameters	Setting values		
	SS-EPI DWI	RS-EPI DWI	FSE-T_2WI
TR/TE [ms]	5000/78	4180/77	5000/78
FOV [mm]		256 × 256	
Matrix size		192 × 192	
Phase direction		A/P	R/L
Slice thickness [mm]		5	
Number of slices		20	
Reduction factor		2	
Echo space [ms]	0.9	0.3	8.6
b-Value [s/mm^2]	0 and 1000	0 and 1000	–
Readout segments	–	5	–

FSE-T_2WI, fast spin-echo T_2-weighted image; RS-EPI DWI, readout segmented-echo planar imaging diffusion-weighted image; SS-EPI DWI, single shot-echo planar imaging diffusion-weighted image.

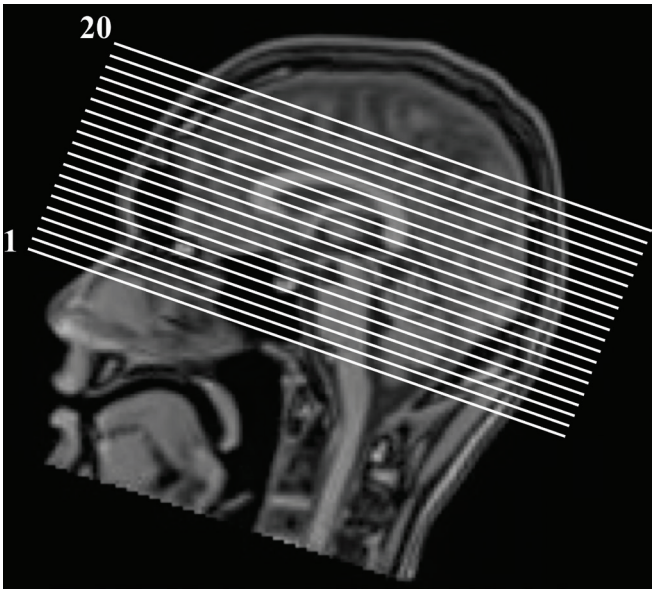

Fig. 1 Example of the slice positioning for the DWI acquisitions used in this study. DWI, diffusion-weighted image.

processing results. Third, 3D labeling was performed and the brain region was extracted as the object with the largest volume. Fourth, binarization was performed, with brain regions assigned a value of 1 and other regions 0. In addition, to take account of defects in the extracted images, we performed an image dilation procedure to expand the extracted area, and created a mask image. The final extracted images (brain SS-EPI DWI, brain RS-EPI DWI, and brain FSE-T_2WI) were obtained by multiplying the original images by the mask images.

Calibration of signal intensity in brain FSE-T_2WI

In each slice of the brain-extracted image data, to reduce the differences in signal intensities, a calibration process equalized the mean value and standard deviation of the signal intensities in the reference image (brain FSE-T_2WI) and that of the source image (*b*0 image of brain SS-EPI DWI) using the following Equation (1):

$$SI_c(x,y) = \frac{\sigma_r}{\sigma_s}\left[SI_s(x,y) - \overline{SI_s}\right] + \overline{SI_r} \quad (1)$$

where $SI_c(x,y)$ is the signal intensity at each pixel of brain FSE-T_2WI after calibration (calibrated FSE-T_2WI), σ_r is the standard deviation of brain FSE-T_2WI, σ_s is the standard deviation of the *b*0 image of brain SS-EPI DWI, $SI_s(x, y)$ is the signal intensity at each pixel of the *b*0 image of brain SS-EPI DWI, $\overline{SI_s}$ is the mean value of signal intensities in the *b*0 image of brain SS-EPI DWI, and $\overline{SI_r}$ is the mean value of signal intensities at the brain FSE-T_2WI. The calculation was performed similarly to the previously reported method.[7]

Nonrigid image registration in SS-EPI DWI

We performed nonrigid image registration using the B-spline method with the *b*0 image of brain SS-EPI DWI as the source image and calibrated FSE-T_2WI as the reference image. The parameters were set as follows: Divergence Weight: 0.0, Curl Weight: 0.0, Landmark Weight: 0.0, Image Weight: 1.0, Stop Threshold: 0.01. Finally, the same deformation as the *b*0 image was applied to the *b*1000 image of brain SS-EPI DWI. We acquired the distortion-corrected DWI using a nonrigid image registration method (corrected brain SS-EPI DWI). This process was done using the Fiji software.[5,8] Calculation time for this process was 13.0 ± 4.4 s per slice.

Evaluation of image distortion in SS-EPI DWI, corrected SS-EPI DWI, and RS-EPI DWI

In order to evaluate the effectiveness of the distortion correction, the mutual information compared with FSE-T_2WI (MI-T_2) was calculated for the *b*1000 images of each brain SS-EPI, corrected brain SS-EPI, and brain RS-EPI according to the previous report.[9] The MI-T_2 was calculated separately for each slice in each DWI volume. First, signal intensities were calibrated to 8-bit gray scale (range: 0–255, bin size = 256) by the following Equation (2) in *b*1000 image of brain SS-EPI DWI, corrected brain SS-EPI DWI, brain RS-EPI DWI, and brain FSE-T_2WI:

$$SI_{post}(x,y) = \mathrm{floor}\left(255\frac{SI_{pre}(x,y) - SI_{min}}{SI_{max} - SI_{min}}\right) \quad (2)$$

where $SI_{post}(x,y)$ is the signal intensity of each MR image at each pixel after 8-bit gray scale calibration process, $SI_{pre}(x,y)$ is the signal intensity of each MR image at each pixel, SI_{min} is the minimum signal intensity of each MR image, and SI_{max} is the maximum signal intensity of each

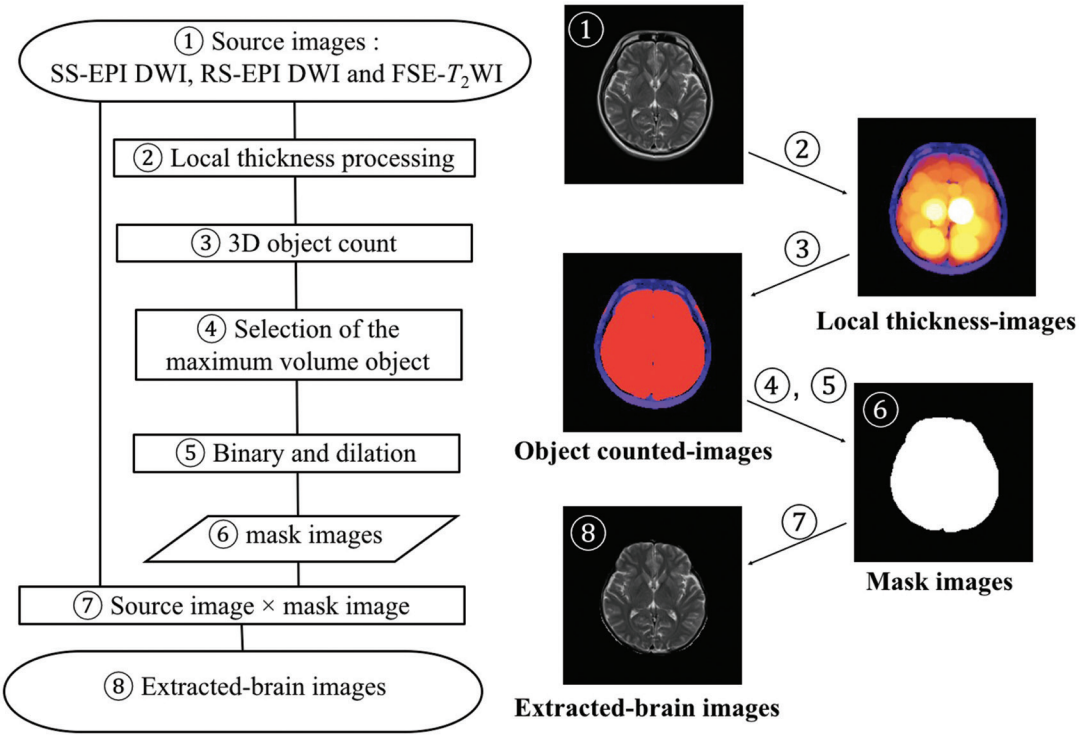

Fig. 2 Schematics of the extraction of the brain region from an image set. FSE-T_2WI, fast spin-echo T_2-weighted image; RS-EPI DWI, readout segmented-echo planar imaging diffusion-weighted image; SS-EPI DWI, single shot echo planar imaging diffusion-weighted image.

MR image. Second, we calculated MI-T_2 using the following Equation (3):

$$\mathrm{MI}-T_2(A,B)=\sum_{i=1}^{256}\sum_{j=1}^{256}p(a,b)\log_2\frac{p(a,b)}{p(a)p(b)} \qquad (3)$$

where MI-T_2 (A, B) is the mutual information of image A (b1000 images of brain SS-EPI DWI, corrected brain SS-EPI DWI, and brain RS-EPI DWI) and B (brain FSE-T_2WI), $p(a, b)$ are 2D histograms (256 × 256) from images A and B, $p(a)$ is the histogram of image A, and $p(b)$ is the histogram of image B. We compared with MI-T_2 of b1000 images of brain SS-EPI (SS-EPI) DWI, corrected brain SS-EPI (corrected SS-EPI) DWI, and brain RS-EPI (RS-EPI) DWI.

The Friedman test with a Nemenyi multiple-comparison test was used to determine statistical significance. R version 3.6.2 (R Foundation for Statistical Computing, Vienna, Austria, http://www.R-project.org/) was used to perform the statistical analysis, and a p-value <0.05 was considered to indicate statistical significance.

Results

Figure 3 shows SS-EPI DWI, corrected SS-EPI DWI, and RS-EPI DWI images at slice positions 3 (a, b, and c), 7 (d, e, and f), and 14 (g, h, and i) from a single subject. Edges derived from the FSE-T_2WI are overlaid in red on the SS-EPI (a, d and g), corrected SS-EPI (b, e and h), and RS-EPI (c, f and i). The arrows indicate regions where the displacement from the red lines appears to be less in the corrected SS-EPI and RS-EPI than in the original SS-EPI.

Table 2 and Fig. 4 show the mean MI-T_2 for each image slice. The corrected SS-EPI or RS-EPI showed higher values than SS-EPI in all slices. The corrected SS-EPI showed the highest values in slice numbers 1–4 and RS-EPI showed the highest values in slices 5–10, with some differences being statistically significant ($p < 0.05$). For slices 11 and above, the corrected SS-EPI showed the highest values, which were significantly higher than values for SS-EPI ($p < 0.05$).

Discussion

MI-T_2 was used to evaluate the image distortion in this study. MI is used as a cost function in image registration, and maximized MI is used for image registration between different imaging modalities (i.e., between CT and MRI).[9] In FSE-T_2WI, there is very little image distortion because the FSE sequence is not subject to a narrow bandwidth in the phase-encode direction. Therefore, we consider that if the MI-T_2 showed a high value, the similarity of an image to the FSE-T_2WI was high, and the image distortion was low. Teruel et al.[10] reported distortion-correction of b0 DWI images using a method based on opposite but symmetrical image distortion with reversed polarity phase-encoding, and showed MI values higher than those of the original DWI. This report supports our findings that the corrected SS-EPI or RS-EPI showed higher MI-T_2 than the SS-EPI. We assume that the degree of MI-T_2 represents the image distortion at each slice in this study.

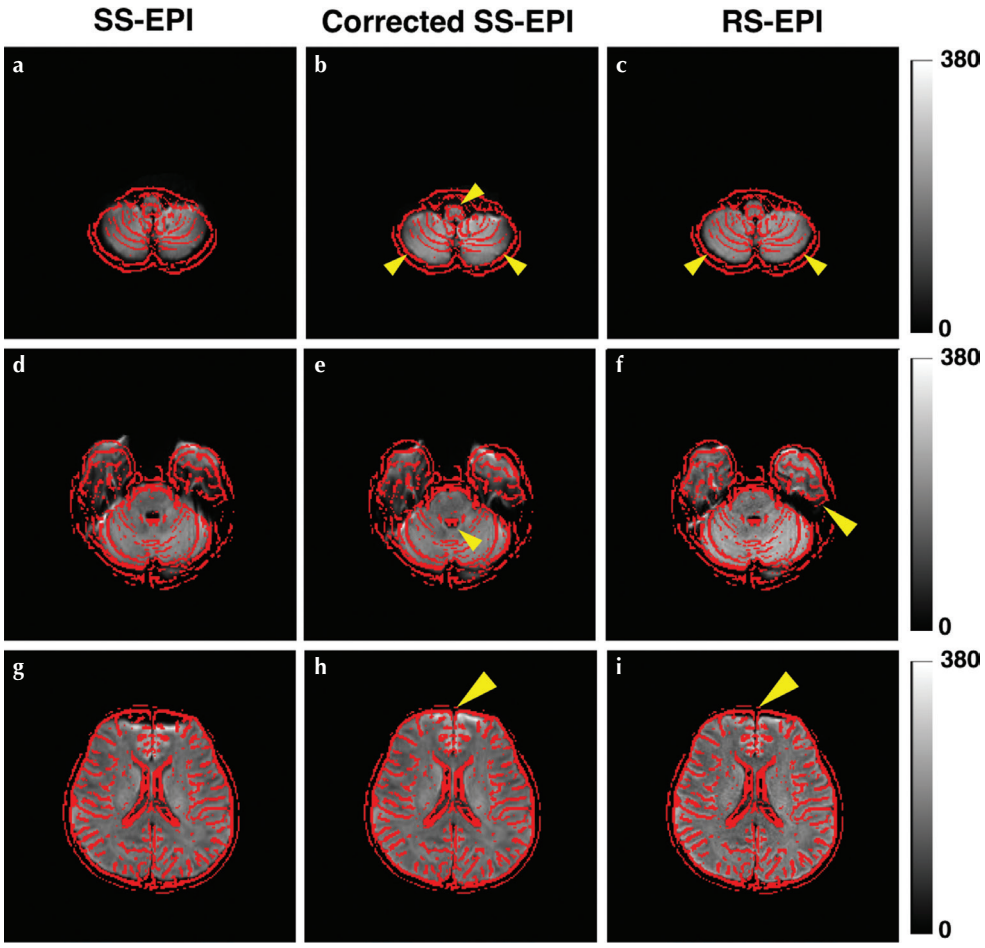

Fig. 3 SS-EPI DWI, corrected SS-EPI DWI, and RS-EPI DWI images from a single subject. Edges from the FSE-T_2WI are overlaid in red on SS-EPI (**a**, **d**, and **g**), corrected SS-EPI (**b**, **e**, and **h**), and RS-EPI (**c**, **f**, and **i**). The displacement from the red line in each corrected DWI is less than that in the SS-EPI (arrows). FSE-T_2WI, fast spin-echo T_2-weighted image; RS-EPI DWI, readout segmented-echo planar imaging diffusion-weighted image; SS-EPI DWI, single shot echo planar imaging diffusion-weighted image.

Nonrigid image registration based on the B-spline method has been previously used for distortion correction in DWI.[4,11] In this method, control points are typically arranged in a grid pattern on source images, and deformations to the source images are performed by moving the points, with B-spline interpolation being used to predict the signal intensity of other points.[8,11] Nonrigid image registration based on the B-spline method was used in this study, and the mean MI-T_2 of the corrected SS-EPI showed higher values than the SS-EPI in all image slices. Therefore, we conclude that effective image distortion-correction was obtained using the nonrigid image registration method in this study.

Treiber et al.[12] reported that severe distortion of brain DWI occurred at the brainstem. Our slice numbers 1–4 corresponded to the inferior cerebellum in each subject. In these slices, the mean MI-T_2 values of the corrected SS-EPI showed the highest values of the three DWI image sets, and the apparent displacement of the brainstem was improved in most subjects (Fig. 3). Moreover, because the difference between the MI-T_2 of RS-EPI and SS-EPI was small, we consider that the image distortion of the SS-EPI was lower in these slices than in other slices. Therefore, the nonrigid image registration method made it possible to largely correct for the image distortion that occurred in the brainstem.

The mean MI-T_2 of RS-EPI showed higher values than the corrected SS-EPI in slice numbers 5–10, corresponding to the pons and midbrain in each subject. Moreover, the mean MI-T_2 of RS-EPI showed significantly higher values than the SS-EPI in slice numbers 7–10. Pronounced image distortion occurred due to B_0 inhomogeneity derived from the air contained in the nasal cavity and the mastoid air cells at these levels. Ardekani and Sinha[4] reported that nonrigid image registration correction of severe image distortion in areas subject to susceptibility artifact areas was limited by the requirement that the Jacobian of the deformation field be positive. Therefore, we consider that the nonrigid image registration method used in this study might be limited at these slice levels. In comparison with the nonrigid image registration, a technique based on *k*-space trajectory enabling short echo space setting, such as RS-EPI, seems to more effectively reduce image distortion and artifacts at these levels.

The mean MI-T_2 of corrected SS-EPI was significantly higher than that of SS-EPI at slice number 11 and above ($p < 0.05$). These slices corresponded to the basal ganglia,

Table 2 Mean values of MI-T_2 at each slice in the SS-EPI DWI, corrected SS-EPI DWI, and RS-EPI DWI

Slice number	MI-T_2 (mean ± S.D.)		
	SS-EPI	Corrected SS-EPI	RS-EPI
1	0.50 ± 0.11	0.55 ± 0.09	0.52 ± 0.10
2	0.61 ± 0.03	0.63 ± 0.04	0.61 ± 0.05
3	0.65 ± 0.03	0.68 ± 0.04	0.64 ± 0.04
4	0.81 ± 0.08	0.87 ± 0.08*	0.83 ± 0.08
5	0.94 ± 0.12	0.97 ± 0.14	0.99 ± 0.12
6	0.99 ± 0.07	1.04 ± 0.08	1.05 ± 0.04
7	1.05 ± 0.02	1.09 ± 0.03*	1.10 ± 0.04*
8	1.14 ± 0.06	1.16 ± 0.07	1.20 ± 0.08*
9	1.11 ± 0.06	1.16 ± 0.05	1.19 ± 0.04*
10	1.18 ± 0.06	1.24 ± 0.07	1.27 ± 0.06*
11	1.21 ± 0.05	1.29 ± 0.06*	1.27 ± 0.05*
12	1.24 ± 0.03	1.31 ± 0.03*	1.28 ± 0.05
13	1.26 ± 0.04	1.33 ± 0.06*	1.32 ± 0.05*
14	1.28 ± 0.05	1.37 ± 0.04*	1.36 ± 0.06*
15	1.27 ± 0.07	1.37 ± 0.08*	1.34 ± 0.07
16	1.24 ± 0.04	1.32 ± 0.05*	1.30 ± 0.05
17	1.25 ± 0.04	1.34 ± 0.03*	1.31 ± 0.04
18	1.23 ± 0.04	1.33 ± 0.04*	1.31 ± 0.05*
19	1.18 ± 0.07	1.29 ± 0.07*	1.25 ± 0.07
20	1.07 ± 0.08	1.19 ± 0.09*	1.14 ± 0.08

*Significant difference versus SS-EPI; Nemenyi test after Friedman's test, $P < 0.05$. MI, mutual information; RS-EPI, readout segmented-echo planar imaging; SS-EPI, single shot-echo planar imaging.

lateral ventricles, and centrum semiovale levels in all subjects. A previous report related to nonrigid image registration methods showed that distortion correction was achieved at these slice levels.[4] This report supports our finding that the mean MI-T_2 of the corrected SS-EPI showed high values at the levels of the basal ganglia and lateral ventricles. At the centrum semiovale level, there are no air cavities such as nasal sinuses that cause severe magnetic susceptibility-related image distortions. Therefore, we consider that the calculational limitations of the nonrigid image registration method were not met at this level, and the nonrigid image registration could adequately correct the image distortion in these images.

If the nonrigid image registration acts to effectively correct the image distortion in image slices where the image distortion is reduced by RS-EPI, it may be possible to reduce the distortion in images acquired on MRI scanners where RS-EPI is not implemented. Moreover, when SS-EPI DWI and FSE-T_2WI are acquired in an examination, the image distortion on the SS-EPI DWI can be corrected using the nonrigid image registration method, without extending the total scan time.

There are some limitations to this study. First, the nonrigid image registration used in this study required the setting of several parameters that affected the results of the registration, such as the weight of the regularizing term based on the divergence.[8] To minimize the variation in the registration results across the subjects and to propose a method less dependent on the subject image data, we set these parameters to 0.0 in this study. Second, this study focused on only the normal brains of healthy volunteers. To confirm the characteristics of the nonrigid image registration method, further evaluations need to be performed in patients with pathological brain abnormalities such as cerebrovascular accidents and brain tumors.

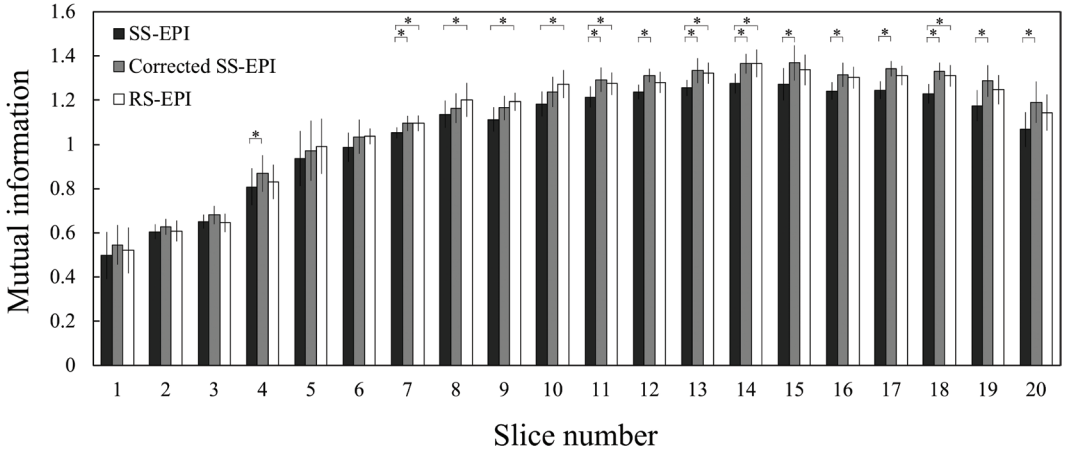

Fig. 4 Mean values of MI-T_2 at each slice in each DWI image set. The corrected SS-EPI showed significantly higher values than the SS-EPI at slice numbers 4, 7, 11 and above ($P < 0.05$). The RS-EPI showed significantly higher values than SS-EPI at slice numbers 7–11, 13, 14, and 18. DWI, diffusion-weighted image; MI, mutual information; RS-EPI, readout segmented-echo planar imaging; SS-EPI, single shot-echo planar imaging.

Conclusion

To evaluate the effectiveness of a nonrigid image registration method, we compared SS-EPI DWI before and after application of nonrigid image registration methods and RS-EPI DWI. The effectiveness of the nonrigid image registration method varied according to the level of the image slices, and distortion-corrected images could be obtained at the level of the basal ganglia, lateral ventricles, and centrum semiovale without using RS-EPI.

Acknowledgment

We thank Edanz Group Japan (www.edanzediting.com/ac) for editing drafts of this manuscript.

Conflicts of Interest

The authors have no conflicts of interest to declare.

References

1. Schaefer PW. Applications of DWI in clinical neurology. J Neurol Sci 2001; 186:S25–S35.
2. Holdsworth SJ, Yeom K, Skare S, Gentles AJ, Barnes PD, Bammer R. Clinical application of readout-segmented-echo-planar imaging for diffusion-weighted imaging in pediatric brain. AJNR Am J Neuroradiol 2011; 32: 1274–1279.
3. Porter DA, Heidemann RM. High resolution diffusion-weighted imaging using readout-segmented echo-planar imaging, parallel imaging and a two-dimensional navigator-based reacquisition. Magn Reson Med 2009; 62:468–475.
4. Ardekani S, Sinha U. Geometric distortion correction of high-resolution 3 T diffusion tensor brain images. Magn Reson Med 2005; 54:1163–1171.
5. Schindelin J, Arganda-Carreras I, Frise E, et al. Fiji: an open-source platform for biological-image analysis. Nat Methods 2012; 9:676–682.
6. Dougherty RP, Kunzelmann KH. Computing local thickness of 3D structures with ImageJ. Microsc Microanal 2007; 13:1678–1679.
7. Tachinaga S, Hiura Y, Kawashita I, Okura Y, Ishida T. Development of a computer-aided diagnostic system for detecting multi sclerosis using magnetic resonance images. Nihon Houshasen Gijutu Gakkai Zasshi 2014; 70:223–229. (in Japanese)
8. Sorzano CO, Thévenaz P, Unser M. Elastic registration of biological images using vector-spline regularization. IEEE Trans Biomed Eng 2005; 52:652–663.
9. Maes F, Collignon A, Vandermeulen D, Marchal G, Suetens P. Multimodality image registration by maximization of mutual information. IEEE Trans Med Imaging 1997; 16:187–198.
10. Teruel JR, Fjøsne HE, Østlie A, et al. Inhomogeneous static magnetic field-induced distortion correction applied to diffusion weighted MRI of the breast at 3T. Magn Reson Med 2015; 74:1138–1144.
11. Glodeck D, Hesser J, Zheng L. Distortion correction of EPI data using multimodal nonrigid registration with an anisotropic regularization. Magn Reson Imaging 2016; 34:127–136.
12. Treiber JM, White NS, Steed TC, et al. Characterization and correction of geometric distortions in 814 diffusion weighted images. PLoS ONE 2016;11:e0152472.